Crack-bridging behaviour of AR-glass multifilament yarns embedded in cement-based matrix – Modelling of ageing effects

M. Butler, V. Mechtcherine
Institute o f Construction Materials, Helmholtzstrasse 10,
TU Dresden, 01062 Dresden, Germany

ABSTRACT

This paper deals with causes for age-dependent changes in mechanical performance of TRC on meso and micro level. The mechanical characteristics of bond between alkali resistant multi-filament yarn and different cementitious matrices before and after accelerated aging were investigated by means of double sided yarn pullout tests. Depending on binder components the yarn pullout behaviour (and with that TRC performance) differs widely with increasing age. Performance losses are caused mainly by microscopic densifications in the interphase between fibre and matrix. This leads to increased bond intensity and restricted slip-ability of filaments. These structure phenomena on micro level were related to the composite behaviour on meso level by means of a phenomenological bond model. The model describes the crack-bridging effect of the multi-filament yarn on single filament level. Thereby each filament possesses a specific deformation length depending on its position in the yarn cross-section and on bond characteristics to the matrix. The deformation lengths can vary if the composite ages. In this way micro structural changes in the composite can be represented by characteristic values of the model. The characteristic values were computed from load-crack width curves obtained in yarn pullout tests.

KEYWORDS

Textile reinforced concrete, multifilament yarn reinforcement, crack bridging, ageing effects

INTRODUCTION

Textile-reinforced concrete (TRC) is a composite construction material consisting of high performance, multifilament yarns of glass or carbon fibre embedded in a matrix of fine-grained concrete. The main features of TRC are its high tensile strength and its pronounced ductile behaviour. TRC can be applied both in the fabrication of new structures and in the strengthening and repair of structural elements made of reinforced concrete or other traditional materials as well [1].

In most of these applications the high tensile strength and toughness of TRC should not degrade significantly with increasing age. Changes in the mechanical performance of the composite can result from deterioration of the armouring AR-glass fibres themselves due to the attack of OH^--ions in the pore solution [2, 3, 4], the static fatigue of the glass fibre under sustained load in the highly alkaline environment [5, 6, 7, 8], and changes in the bond between matrix and fibres [9, 10, 11, 12].

In this project the contribution of individual damage mechanisms to degradation of crack-bridging behaviour of multifilament yarn and their interaction is shown by means of a simple phenomenological model. The model is based on experimental data achieved from multifilament yarn pullout testing and micro-structural investigation of the yarn-matrix interface. A more extended and detailed presentation of the research is given in [13].

EXPERIMENTS – MATERIALS, METHODS, RESULTS

Materials – yarn and fine-grained concrete

Multifilament yarn made of AR-glass (type CEM-FIL) was used as reinforcing material in the pullout tests. The multifilament yarn consists of 1600 individual filaments with a mean diameter of 13.6 µm. The mean tensile strength of such filaments is 1917 MPa and their mean strain capacity 0.0258.
A fine-grained concrete (composition: CEM I 32,5 R – 557 kg/m³, fly ash – 251 kg/m³, microsilica – 56 kg/m³, sand 0/1 mm – 1114 kg/m³, water – 251 kg/m³) was used as matrix material. Compared to ordinary concrete the mixture has high binder content. In this matrix the appearance of $Ca(OH)_2$ (abbrev.: CH) and alkalis is controlled due to the presence of fly ash and microsilica in the binder.

Test method – double-sided yarn pullout

The crack-bridging performance of multifilament yarn was evaluated in double-side pullout tests. Doubly symmetrical, bone shaped prisms featuring a notch of depth 1mm in the middle were used as specimens. Each specimen was reinforced with three parallel oriented multifilament yarns extending over the entire length of the specimen. The amount of reinforcement was chosen in such way that multiple cracking was avoided and only single-crack formation at the notch occurred, cf. [13, 14].
After demoulding one day after fabrication all specimens were stored for 6 days in water (20°C). Subsequently, one small part of specimens was subjected to reference storage (20°C/65% RH) until testing at an age of 28 days. The main part of the test specimens was subjected to accelerated ageing in a fog room (40°C/99% RH). The periods of fog room storage were 28, 56, 90, 180 and 360 days.
The pullout testing was performed under controlled deformation conditions defined by a crack opening rate of 1mm/min, cf. [13, 14].

Results of double-sided pullout tests and micro-structural investigations

Figure 1 shows the characteristic pullout curves. Each curve depicted represents a best-fit curve based on at least 7 individual pullout curves. The pullout curves are represented in simplified fashion. The curve branches describing the uncracked state of specimens are neglected and replaced by an interpolated line from $F(w=0) = 0$ to the point where the yarn pullout is initiated, just after cracking of matrix, cf. [13, 14]. Likewise, the representation of the x-axis is simplified. It is not divided into axis intercepts for strain as well as for crack opening. Therefore the crack opening $w = 0$ is shifted to the left at the point where $F = 0$.
With increasing duration of accelerated ageing the maximum fibre pullout force decreases by approx. 40% after 360 days of accelerated ageing, whilst the pullout work during crack opening decreases by approx. 60% compared to the reference specimen. The tendency to decrease the maximum pullout force as well as pullout energy is more distinct in early ageing states than at higher composite age.
Figure 2 represents the characteristic microstructure in the interface between the multifilament yarn's sleeve filaments and matrix after 28 days' reference storage. The single filaments are embedded in an inhomogeneous matrix consisting of un-hydrated binder particles and hydration products. The matrix shows a structure which is not yet very dense. Contact between the hydration products and the filament surface is visible only at discrete points. Due to the ongoing hydration process during ageing the matrix becomes denser. The single filaments are covered by mineral incrustations mainly consisting of CSH phases. This leads to hydration products on filament surface which are much denser compared to Figure 2 and enclose the filament surface nearly on the entire surface, cf. [13, 14].

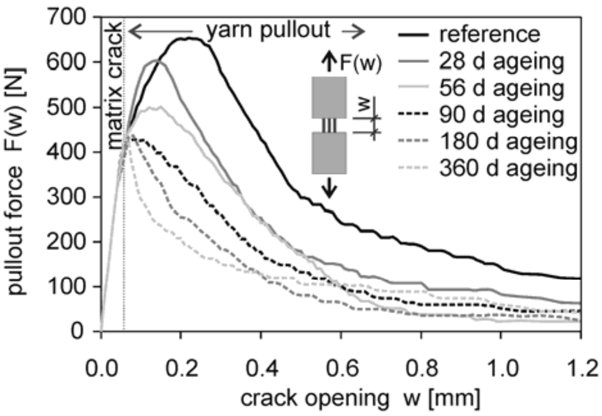

Fig. 1: Force vs crack opening curves; storage at 40°C / 99% RH, reference at 20°C / 65% RH.

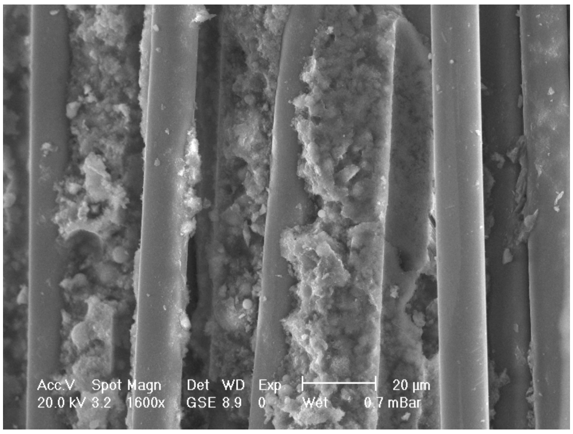

Fig. 2: ESEM image of AR glass filaments in matrix M1, 28 days of reference storage (20°C / 65% RH)

ADHESIVE CROSS-LINKAGE MODEL

Phenomenological basics of the model

The bond between filament and cementitious matrix is non-uniform. The hydration products form adhesive cross-links between matrix and filament or filament and filament, respectively (cf. Figure 2). The bond properties of the cross-links depend on the characteristics of hydration products, which are influenced by the binder composition, the filament-sizing, and the condition and duration of hydration, e.g. [13]. However, the cross-links reduce or prevent the displacement of the filaments, e.g. [12].

The basic idea of the adhesive cross-linkage model was proposed by Schorn [15] and is based on the assumption that between two cross-links the filament can be deformed along the so-called available deformation length L_0. In Figure 3 different types of bonding between filament and matrix and therefore different available deformation lengths are shown. Due to the shear stiffness of adhesive cross-links and the linkage between filaments, an effective deformation length L_W is educed, exceeding the available deformation length L_0 of the filament (cf. Figure 3b). In the following the term “deformation length” is used synonymously with “effective deformation length”.

Distribution of deformation lengths

The frequency of cross-links decreases significantly from the sleeve filaments to the inner filaments. This is caused by the tiny distances between the filaments. The relatively large binder particles can not penetrate into the inner part of the multifilament yarn, only hydration products can reach yarn’s core.

According to the cross-link model each filament has a specific deformation length depending on its position in the cross section of the yarn. In Figure 4 (left) a possible arrangement of deformation lengths over yarn diameter is sketched. To model the crack-bridging behaviour of multifilament yarn, the indication of the deformation lengths of all filaments in the yarn becomes necessary. Figure 4 (right) illustrates a possible distribution of deformation lengths L_W. Here the filaments are sorted according to their deformation lengths independent of position in the yarn.

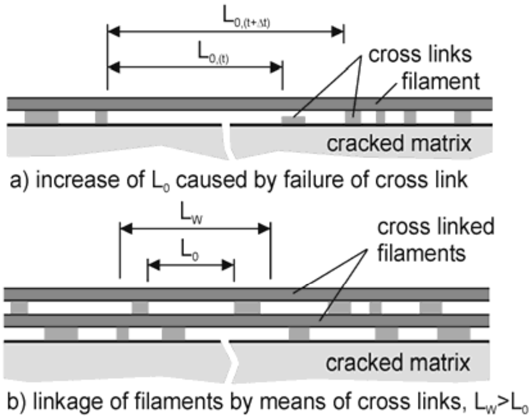

Fig. 3: Different types of bonding represented by different deformation lengths of filaments

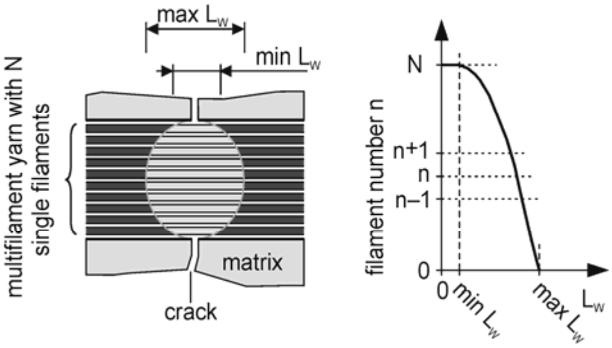

Fig. 4: Arrangement of deformation lengths over diameter of yarn (left) and their distribution over filament number (right)

Modelling the yarn's crack-bridging behaviour

The filament stress at defined crack openings can be calculated according to Equation 1 where σ = stress; E = young's modulus; L_W = deformation length of the filament, and w = crack width.

$$\sigma_n = E_n \varepsilon_n = E_n \frac{w}{L_{Wn}} \tag{1}$$

With increasing crack width w, the filaments fail little by little when each individual filament's strength is exceeded according to its deformation length. The stress level σ in a filament increases with decreasing L_W for a given crack-opening. Furthermore, cross-links can fail if their shear strength is exceeded before the maximum filament stress is reached. In this case, the associated L_W increases. The crack-bridging load transferred by the entire multifilament yarn across the crack at given crack width w can be determined according to Equation 2 where F = crack-bridging force; A = cross section of filament; N = total number of filaments; and n_f = number of failed filaments.

$$F = \sum_{n=1}^{N-n_f} F_n = \sum_{n=1}^{N-n_f} \sigma_n A_n = \sum_{n=1}^{N-n_f} A_n E_n \frac{w}{L_{Wn}} \tag{2}$$

In Figure 5 (left) a linear distribution of deformation lengths $L_w(n)$ is indicated. At the yarn's core 10% of filaments are assumed inactive in crack-bridging load transfer; also cross-link failure is excluded. In Figure 5 (right) the resulting filament stresses, the crack-bridging load, and the number of failed filaments are indicated for crack width of $w = 0.5w_{max}$.

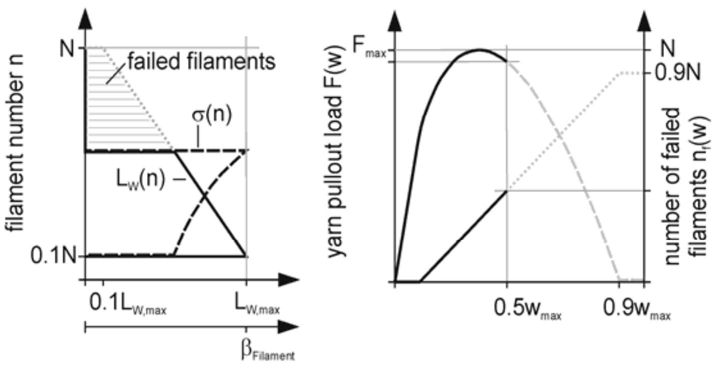

Fig. 5: Deformation lengths of filaments L_W, filament stress σ, yarn pullout load F and number of failed filaments n_f for crack width $w = 0.5w_{max}$.

Recursive determination of distribution of deformation lengths

The adhesive cross-linkage model enables a specific correlation between the bonding situation of a multifilament yarn and its mechanical behaviour when bridging a single crack. For computation of a load-crack width curve, knowledge of the distribution of the filaments' deformation lengths is indispensable. But the experimental determination of position, strength, and stiffness of cross-links is nearly impossible. The cross-links haven't an exact physical counterpart; they are rather an idealised abstraction of several bonding phenomena.

However, the distribution of deformation lengths can be computed based on experimental data observed in pullout tests. At begin of the recursive calculation process is assumed that all filaments have failed at crack width $w_{max} = w_U$. The number of intact filaments $M_U = 0$. No load is transmitted over the crack: $F_U = 0$. This initial state is summarised in Equation 3:

$$w = w_{\max} = w_U \;;\; F_U = M_U = 0 \;;\; L_W = L_{W,\max} = L_{W,V} \tag{3}$$

Before the state according to Equation 3 is reached, at crack width w_{U-1}, a load F_{U-1} is transferred through M_{U-1} filaments. The deformation length of these filaments is $L_{W,V-1}$. If Young's modulus E and the cross section A of load bearing filaments are known, their total number can be calculated according Equations 4 and 5:

$$w = w_{U-1} : F_{U-1} = E_F A_F \frac{w_{U-1}}{L_{W,V-1}} m_{U-1} \tag{4}$$

$$\rightarrow \quad m_{U-1} = M_{U-1} = \frac{F_{U-1}}{E_F A_F w_{U-1}} L_{W,V-1} \tag{5}$$

Reducing the crack width by a further decrement at w_{U-2}, the crack-bridging load is F_{U-2}. The total number of intact filaments M_{U-2} is composed of the number of filaments m_{U-1} (which stay un-cracked until crack width w_{U-1}) and the number of filaments m_{U-2} which fail during crack opening from w_{U-2} to w_{U-1} (cf. Figure 6). At this point F_{U-2} results from the particular straining of both groups of filaments, m_{U-1} and m_{U-2}, respectively; see Equation 6. Considering the results of Equation 5, m_{U-2} can now be calculated according to Equation 7:

$$w = w_{U-2} : F_{U-2} = E_F A_F \left(\frac{w_{U-2}}{L_{W,V-1}} m_{U-1} + \frac{w_{U-2}}{L_{W,V-2}} m_{U-2} \right) \tag{6}$$

$$\rightarrow \quad m_{U-2} = \left(\frac{F_{U-2}}{E_F A_F w_{U-2}} - \frac{m_{U-1}}{L_{W,V-1}} \right) L_{W,V-2} \tag{7}$$

$$M_{U-2} = m_{U-1} + m_{U-2} \tag{8}$$

At any crack width w_{U-i}, where ($U > i > 1$), the crack-bridging load F_{U-i} is composed of i individual load components, resulting from m strained filaments inside each filament group (Equation 9, Figure 6). The number of filaments m_{U-i} failing during crack opening from w_{U-i} to w_{U-i+1} can be calculated according to Equation 10 and the total number of intact filaments M_{U-i} according Equation 11:

$$w = w_{U-i} : F_{U-i} = E_F A_F \left(\frac{w_{U-i}}{L_{W,V-1}} m_{U-1} + \frac{w_{U-i}}{L_{W,V-2}} m_{U-2} + \cdots + \frac{w_{U-i}}{L_{W,V-i+1}} m_{U-i+1} + \frac{w_{U-i}}{L_{W,V-i}} m_{U-i} \right) \tag{9}$$

$$\rightarrow \quad m_{U-i} = \left(\frac{F_{U-i}}{E_F A_F w_{U-i}} - \sum_{k=1}^{i-1} \frac{m_{U-k}}{L_{W,V-k}} \right) L_{W,V-i} \tag{10}$$

$$M_{U-i} = m_{U-1} + m_{U-2} + \cdots + m_{U-i+1} + m_{U-i} = \sum_{k=1}^{i} m_{U-k} \tag{11}$$

To calculate the number of filaments m_{U-i} the specification of the deformation length of filaments $L_{W,V-i}$ is indispensable. This definition is based on the failure strain of filaments as shown in Equation 12, where $\varepsilon_{F,f}$ = failure strain of filaments.

$$\varepsilon_{F,f} = \frac{w_{U-i}}{L_{W,V-i}} \quad \rightarrow \quad L_{W,V-i} = \frac{w_{U-i}}{\varepsilon_{F,f}} \tag{12}$$

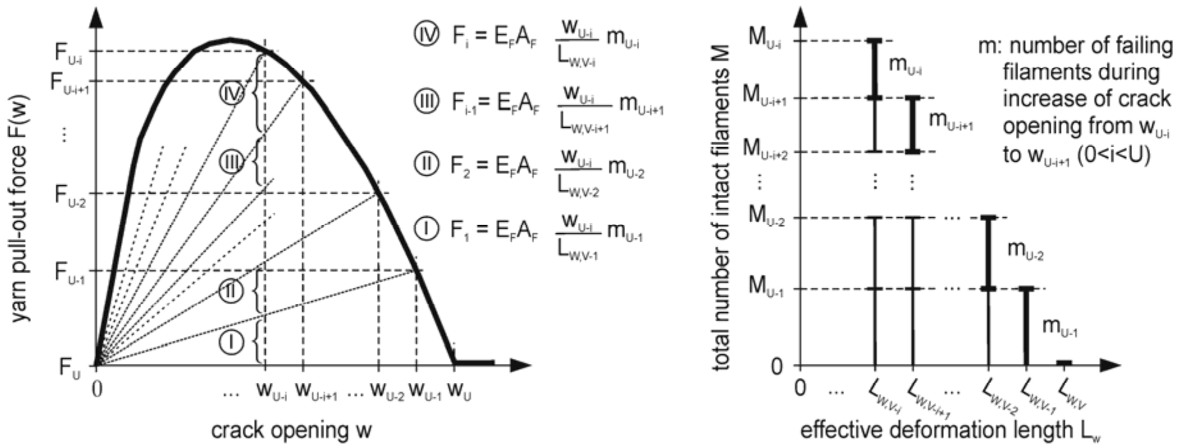

Fig. 6: Sketch of calculation process of recursive determination of distribution of filament's deformation lengths based on measured pullout load-crack width curve.

The set of pair of values ($L_{W,V-i}$; M_{U-i}) represents the distribution of the filaments' deformation lengths inside the multifilament yarn bridging a single crack. To enable a graphic representation similar to Figure 4 (right) the distribution-curve based on discrete pair of values ($L_{W,V-i}$; M_{U-i}) is transformed via linear interpolation to a quasi-continuous distribution curve based on pairs of values ($L_{W,V-i}$; n_j), where n = individual filament number.

A calculated total number of filaments N_{calc} results from this numerical processing. In the specimen the number of inactive filaments N_P can be determined by counting the filaments, which are pulled-out completely. Comparing $N_{calc} + N_P$ and the physical number of filaments in the yarn N, three cases must be distinguished:

a) $N_{calc} + N_p < N$: An iterative recalculation of $L_W(n)$ is performed with the stepwise reduced failure strain of filaments $\varepsilon_{F,f}$ until the condition $N_{calc} + N_p = N$ is satisfied. This case indicates a loss of filament strength, according to the reduction of $\varepsilon_{F,f}$.

b) $N_{calc} + N_p = N$: The calculation can be completed.

c) $N_{calc} + N_p > N$: The condition $N_{calc} + N_p = N$ can not be satisfied. This indicates a cross-link breakdown instead of filament failure. The number of excessive filaments $N - (N_{calc} + N_p)$ and their deformation lengths indicate to what extent the breakdown of cross-links occurs [13].

APPLICATION OF THE CALCULATION MODEL ON EXPERIMENTAL RESULTS

The method of recursive calculation of distribution of deformation lengths was used to conclude from experimental results to the bonding situation inside the multifilament yarn. Based on the results as pictured in Figure 1 a distribution curve of deformation lengths $L_W(n)$ was computed for each simplified pullout-crack width curve. Figure 7 shows the resulting $L_W(n)$-curves. Additionally the filament strengths β_F are indicated, which were used to calculate these curves. During ageing a decrease in the deformation lengths of almost all filaments can be reported. The minimal deformation length $L_{W,min}$ at filament number n = 4800 is reduced from 7.5mm (reference curve) to 2mm (56d ageing). These reductions happen mainly in the sleeve filaments. Only the deformation lengths of core filaments (n = 1 ··· approx. 300) show nearly no change with increasing age. From this state of ageing until an age of 360 days, the filament strength used in calculation was reduced from 1917MPa to 1451MPa to satisfy the condition $N_{calc} + N_p = N = 4800$. Only in reference specimens and after 28 days accelerated ageing higher numbers of filaments $N_{calc} + N_p$ were determined than were physically present in the yarn ($N = 4800$).

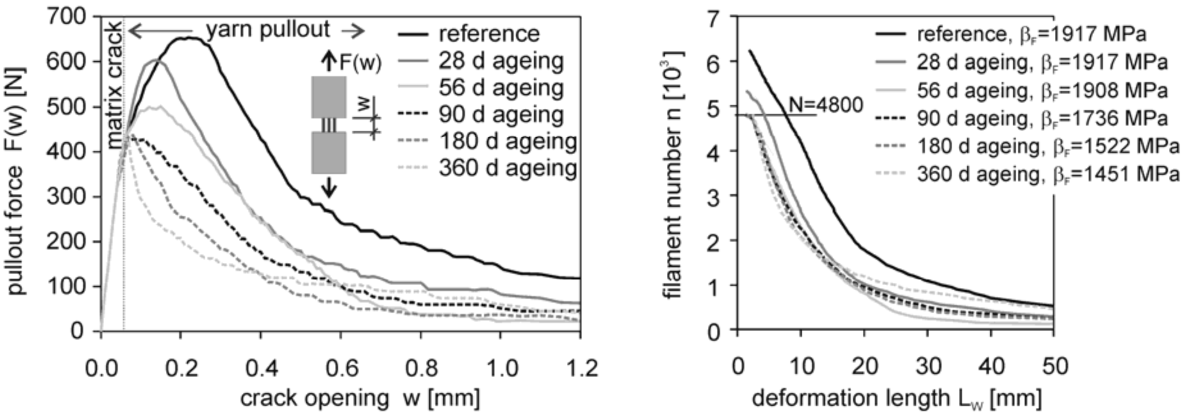

Fig. 7: Calculated distribution of filament deformation lengths for matrix M1 specimens (based on Figure 1; repeated representation at left hand side).

DISCUSSION OF EXPERIMENTAL AND NUMERICAL RESULTS

At this section the results of mechanical testing, of numerical modelling, and of micro-structural investigation will be discussed with a view to identifying the mechanisms which lead to the degradation in crack-bridging behaviour of multifilament yarn during ageing.

The reference specimens show favourable pullout behaviour. The well developed bond between filaments and matrices enables the slip of filaments relative to the matrix at high filament stress levels instead of filament failure and with that a high pullout work. This is substantiated by the distribution of deformation lengths, which indicate a significant potential for cross-link breakdown of reference specimen (cf. Figure 7).

The tested specimens show a pronounced degradation of mechanical performance with age. During hydration process tiny slender CSH phases as well as relatively large and splittable CH phases are produced. A part of CH is transformed during pozzolanic reaction to CSH phases featuring a different morphology than CSH resulting from clinker hydration. Around the filament surfaces these hydration products initially form thin-walled, slender wrappings, which become increasingly compact and stiffer, producing inflexible crusts. The rapid densification process in the matrix-filament interface with increasing age is substantiated by rapidly decreasing deformation lengths (Figure 7). Thus, failure strain of the filaments is reached at smaller crack widths. Also the crusts restrict the slip of filaments in the vicinity of a matrix crack (no potential for cross-link breakdown from 56 day ageing, Figure 7).

Furthermore, these brittle crusts can flake off locally if the covered filament is strained. At the points where the cross-section changes from a “composite-type”, consisting of filament and enveloping crust, to the original filament, high stress concentrations can arise due to the notch effect, which leads to the premature failure of the filament. This effect is represented by reduced strength of filaments β_F (cf. Figure 7). Also, local notching of filament surface due to the growth of surface flaws [7, 8] can not excluded. These multiple effects explain the decrease in performance of aged specimens.

CONCLUSIONS

The degradations in mechanical performance of crack-bridging multifilament yarns are mainly caused by changes in the microstructure in the interface between matrix and fila-

ments and between the filaments themselves, respectively. This could be evidenced by micro-structural investigations of interface morphology as well as by means of modelling the time-dependent changes in distribution of filament deformation lengths $L_W(n)$. This distribution $L_W(n)$ can be computed from experimental pullout data according to a simple phenomenological model. With applicable identification of $L_W(n)$, densifications in the filament-matrix interface can be concluded, which reduce the deformability of filaments, hence causing a precipitate filament failure.
Furthermore, the changes in the morphology can lead to the decrease in filament strength. The causes of losses in the filament strength can be both mechanical notching due to the scaling of mineral incrustations from the filament surface as well as the chemical notching of the filaments' bulk glass, referred to as the less than critical growth of surface flaws. Beside this the potential for cross-link breakdown can be estimated. It is an important composite feature to assure ductile crack-bridging through multifilament yarns at high load level.

REFERENCES

[1] Brameshuber, W. (ed.): Textile Reinforced Concrete. State-of-the-Art Report RILEM Technical Commitee 201-TRC. RILEM Report 36, RILEM Publications S.A.R.L. (2006)
[2] Paul, A.: Chemical durability of glasses; a thermodynamic approach. J Mater Sci 12 (1977) No. 11, pp. 2246–2268
[3] Yilmaz, V.; Glasser, F.: Reaction of alkali-resistant glass fibres with cement. Part 2: durability in cement matrices conditioned with silica fume. Glass Technology 32 (1991) No.4, pp.138–147
[4] Hempel, S.; Butler, M.: Microscopic investigations on durability of textile reinforced concrete. In: Proc. 11th Euroseminar on microscopy applied to building materials, Porto (2007)
[5] Tomozawa, M.: Fracture of glasses. Annu Rev Mater Sci 26 (1996.) pp. 43–74.
[6] Michalske, T.A.; Freiman, S.W.: A molecular mechanism for stress corrosion in vitreous silica. J Am Ceram Soc 66 (1983) No.4, pp. 284–288
[7] Purnell, P.; Short, N.R.; Page, C.L.: A static fatigue model for the durability of glass fibre reinforced cement. J Mater Sci 36 (2001) No.22, pp 5385–5390
[8] Orlowsky, J.; Raupach, M.: Durability model for AR-glass fibres in textile reinforced concrete. Materials and Structures 41 (2008) No.7, pp.1225-1233
[9] Bartos, P.J.M.; Zhu, W.: Effect of microsilica and acrylic polymer treatment on the ageing of GRC. Cement Concrete Compos 18 (1996) No.1, pp. 31–39
[10] Bentur, A.: Role of interfaces in controlling durability of fiber-reinforced cements. J Mater Civil Eng 12 (2000) No. 1, pp. 2–7
[11] Zhu, W.; Bartos, P.J.M.: Assessment of interfacial microstructure and bond properties in aged GRC using a novel microindentation method. Cem Concr Res 27(1997) No.11. pp. 1701–1711
[12] Glinicki, M.A.; Brandt, A.M.: Quantification of glass fibre–cement interfacial properties by SEM-based push-out test. Proc 5th int RILEM workshop high performance fiber reinforced cement composites, Proc 53 RILEM (2007) pp. 343–355.
[13] Butler, M.: Zur Dauerhaftigkeit von Verbundwerkstoffen aus zementgebundenen Matrices und alkaliresistenten Glasfaser-Multifilamentgarnen. Dissertation at the Institute of Construction Materials, TU Dresden (2009), in German
[14] Butler, M., Mechtcherine, V. Hempel, S.: Durability of textile reinforced concrete made with AR glass fibre: effect of the matrix composition. Materials and Structures, DOI: 10.1617/s11527-010-9586-8, in press, (2010).
[15] Schorn, H.: Ein Verbundmodell für Glasfaserbewehrungen im Beton. Bautechnik 80 (2003) No.3, pp. 174-180